New Journal of Physics
The open access journal at the forefront of physics

Deutsche Physikalische Gesellschaft DPG IOP Institute of Physics

PAPER • OPEN ACCESS

Coiling free electron matter waves

To cite this article: J Pierce *et al* 2019 *New J. Phys.* **21** 043018

New Journal of Physics
The open access journal at the forefront of physics

Deutsche Physikalische Gesellschaft DPG
IOP Institute of Physics

Published in partnership with: Deutsche Physikalische Gesellschaft and the Institute of Physics

OPEN ACCESS

RECEIVED
12 February 2019

REVISED
26 March 2019

ACCEPTED FOR PUBLICATION
1 April 2019

PUBLISHED
15 April 2019

PAPER

Coiling free electron matter waves

J Pierce[1], J Webster[2], H Larocque[3], E Karimi[3], B McMorran[1] and A Forbes[2]

[1] Department of Physics, University of Oregon, 1585 E 13th Avenue, Eugene, OR 97403, United States of America
[2] School of Physics, University of the Witwatersrand, Private Bag 3, Wits 2050, South Africa
[3] Department of Physics, University of Ottawa, 25 Templeton St., Ottawa, ON K1N 6N5, Canada

E-mail: andrew.forbes@wits.ac.za

Keywords: matter waves, orbital angular momentum, accelerating waves, structured waves

Supplementary material for this article is available online

Abstract

Here we demonstrate particle beams that spiral in free space devoid of external fields. The beams consist of electrons in two lobes that twist around each other along the optical axis, such that each electron can be described by a two-lobed probability distribution that rotates as it propagates. Furthermore, we demonstrate that this twisting distribution can undergo programmed periods of angular acceleration. These unusual states are produced by preparing each free electron wavefunction in a superposition of non-diffracting Bessel modes that carry orbital angular momentum using nanofabricated diffraction holograms. The holograms can encode nonlinear azimuthal phase so that the resulting electron probability distribution twists in space in a controllable manner, accelerating and decelerating during propagation, without any radiation. This work provides a new platform to explore the dynamics of electrons in magnetic fields, and opens the possibility of producing other types of particle beams with coiling geometries.

1. Introduction

Recent work with diffractive electron optics in transmission electron microscopes (TEMs) has allowed for the reliable creation and study of structured electron beams [1]. One such structure is a freely-propagating electron matter wave with a helical phase $e^{i\ell\phi}$, where ℓ is an integer and ϕ is the azimuthal coordinate, winding about the azimuth, called an electron vortex [2–4]. The phase vortex has an associated quantized orbital angular momentum (OAM). Electron beams with OAM-carrying phase vortices result from a long tradition within physics dating back to Dirac or even earlier [5, 6]. The first experimental demonstration of electron vortices was in 2010 by Uchida and Tonomura [7]. Uchida and Tonomura employed a graphite staircase to approximate a spiral phase plate, which is commonly used in optics [8]. Current work utilizing off-axis holograms within a TEM allows for a high degree of control over the structure of a diffracted electron beam [9–12]. Electron vortex beams have applications in numerous scientific studies, including potential magnetic monopole detection [13–15], measuring magnetic properties [16–18], atomic scale resolution techniques [19], and magnetic dichroism experiments [20]. In all these works, it should be noted that the term 'vortex' here denotes the phase of the wavefunction only; not the motion. The movement of an electron vortex probability distribution deviates only slightly from a normal, non-vortex electron beam, and can be described by a collection of straight trajectories with a very slight azimuthal skew between them [6, 21].

Here we create an electron beam with a probability distribution that observably rotates with a controllable angular velocity as it propagates, forming a coil. The particle beam follows a helical trajectory in free space, shown experimentally in figure 1, without interacting with an external force or potential. We achieve this by preparing each electron in the beam in a coherent superposition of quantized orbital states. Nanofabricated diffraction holograms are used to manipulate the phase of electron matter waves such that they are described by combinations of Bessel states with a nonlinear azimuthal phase. The resulting electron matter wave is non-diffracting over a finite range, with a probability density that exhibits local angular acceleration in a controllable

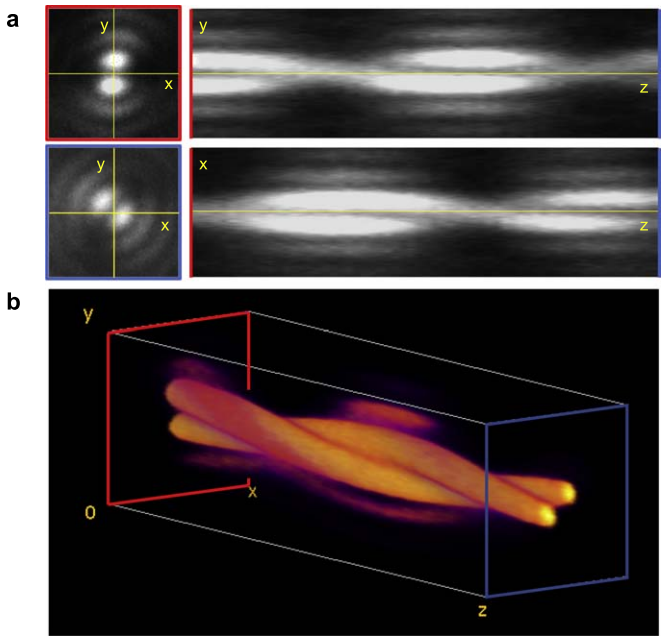

Figure 1. A twisting electron beam. A 3D reconstruction of an experimental electron beam that twists in free space, as show in (a) orthographic and (b) oblique projections. The beam propagates in the $+z$-direction. The beam structure was determined by recording microscopic images of the beam in various x–y planes along z through a focal series, and then reconstructing the 3D structure using interpolation.

manner. The matter wave domain allows us to investigate properties not evident in the optical domain: we study the electrodynamic properties of these angularly accelerating waves and confirm zero radiation (zero Poynting vector) outward from the accelerating charged beam, consistent with the view that the acceleration is local and through interference, while the particle trajectories remain in straight lines even though the wave appears to be spiralling. The motion of the spirally lobes is akin to an artificial magnetic field, but resolved quantum mechanically by a simple model of an electron as an extended wavefunction, thus providing deeper insight into angular motion.

2. Description of coiling electron beams

The coiling electron beams we demonstrate can be described by a combination of four Bessel wavefunctions [12, 22]. A pure Bessel mode is described in cylindrical coordinates (r, ϕ, z) by

$$\psi_{\ell,\alpha}(r,\ \phi,\ z) = J_\ell(kr\sin\alpha)\,\mathrm{e}^{\mathrm{i}kz\cos\alpha}\mathrm{e}^{\mathrm{i}\ell\phi}. \tag{1}$$

This describes a collection of plane waves with wavenumber $k = \sqrt{2mE}/\hbar$ all converging along the optical axis in a cone of semi-angle α, such that the radial and longitudinal components of the wavevector are given by $k_r = k\sin\alpha$ and $k_z = k\cos\alpha$, respectively. The amplitude of the wave is described by a Bessel function J_ℓ, where the topological charge ℓ gives rise to an OAM of $\ell\,\hbar$ per electron. For a single Bessel mode, the phase varies linearly by $2\pi\ell$ about the azimuth, and is referred to as a canonical vortex field [23].

A superposition of Bessel states of opposite helicities and different convergence angles creates angularly rotating and accelerating electron waves:

$$\psi_{\mathrm{acc}}(r,\ \phi,\ z) = \psi_{\ell,\alpha_1}(r,\ \phi,\ z) + \psi_{-\ell,\alpha_2}(r,\ \phi,\ z) + D[\psi_{-\ell,\alpha_1}(r,\ \phi,\ z) + \psi_{\ell,\alpha_2}(r,\ \phi,\ z)], \tag{2}$$

where D is a real parameter between 0 and 1, referred to as the anisotropic parameter. The difference in convergence angles, α_1 and α_2, gives rise to angular rotation of the wave. This can most readily be seen in the simplest of case where $D = 0$, in which the states are defined by a balanced superposition of canonical vortices. In this case, the total wavefunction becomes proportional to $\exp(\mathrm{i}\ell\phi + \mathrm{i}k_{z1}z) + \exp(-\mathrm{i}\ell\phi - \mathrm{i}k_{z2}z) \propto \cos(\ell\phi - \Delta k_z z)$. As illustrated in figure 2 (a), this state is defined by a petal structure rotating at a constant rate [24–27] with propagation distance, given by $\dot{\phi} = \Delta k_z/\Delta\ell$.

When the anisotropic parameter is non-zero ($D > 0$), the rate at which the wavefunction's petal structure rotates begins to vary upon propagation [28–30], thus resulting in an angularly accelerating and decelerating electron wave, as shown in figures 2(b), (c). The dynamics of this wavefunction can be more easily grasped when equation (2) is rearranged into the following form

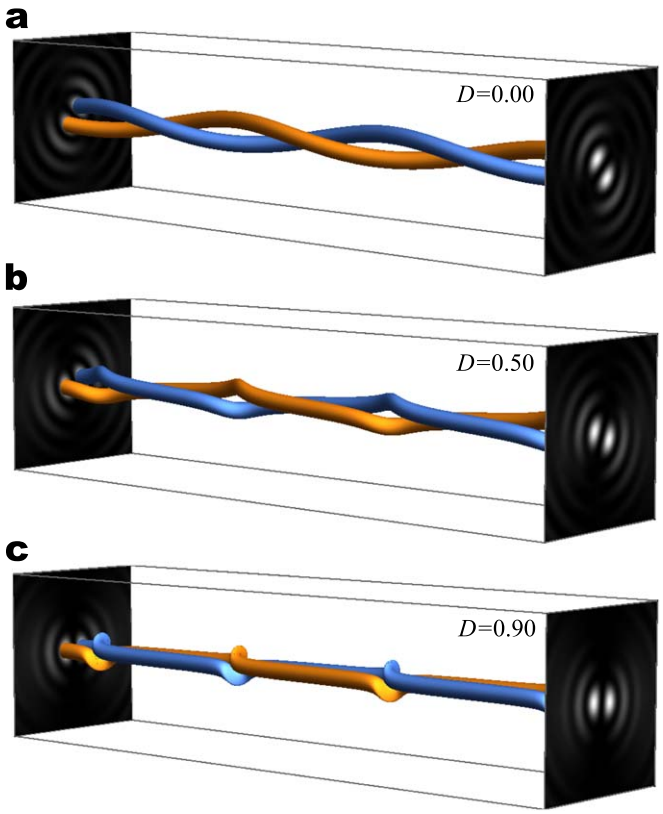

Figure 2. Angular rotating waves. Three-dimensional representations of the angular rotation upon propagation of the electron waves as described by equation (2) and equation (3) for $\ell = 1$. (a) When $D = 0$ the wave rotates during propagation at a constant angular velocity, while for increasing D the wave accelerates and decelerates, tightening the twisted motion, as shown in (b) and (c). The colored tubes track the locations of the inner petal-like structure of the wave, i.e. the two lobes formed by $|\psi_{\rm acc}|^2$.

$$\psi_{\rm acc}(r,\,\phi,\,z) = \left(1 + \frac{2D\cos(2\ell\phi)}{1+D^2}\right)^{\frac{1}{2}} e^{i\bar{k}_z z}[\mathcal{J}^{+}_{\ell}(r)\cos(\Delta k_z z + \ell\varphi_{\ell}(\phi)) + i\mathcal{J}^{-}_{\ell}(r)\sin(\Delta k_z z + \ell\varphi_{\ell}(\phi))], \quad (3)$$

where $\mathcal{J}^{\pm}_{\ell}(r) = J_{\ell}(k_{r1}r) \pm J_{\ell}(k_{r2}r)$, $\bar{k}_z = (k_{z1} + k_{z2})/2$, and $\Delta k_z = (k_{z1} - k_{z2})/2$. Here we see that the anisotropic parameter D introduces a nonlinear variation of the azimuthal phase profile $\varphi_{\ell}(\phi)$ of the wavefunction given by

$$\varphi_{\ell}(\phi) = -\phi + \frac{1}{\ell}\arctan\left(\frac{\sin(2\ell\phi)}{\cos(2\ell\phi) + D}\right). \quad (4)$$

To demonstrate the accelerating motion of this state, we set the phase terms $\Delta k_z z + \ell\varphi_{\ell}(\phi)$ to a constant which in turn allows us to track any point of interest within our wavefunction, for example, one of the petals as tracked in figure 2. From this we find that the rotation (Φ), angular velocity ($\partial_z\Phi$), and angular acceleration ($\partial_z^2\Phi$) as a function of the propagation distance are given by

$$\Phi(z) = -\frac{1}{\ell}\arctan\left(\frac{1+D}{1-D}\tan(\Delta k_z z)\right), \quad (5)$$

$$\partial_z\Phi(z) = -\frac{\Delta k_z}{\ell}\frac{1-D^2}{1+D^2-2D\cos(2\Delta k_z z)}, \quad (6)$$

$$\partial_z^2\Phi(z) = -\frac{\Delta k_z^2}{\ell}\frac{4D(D^2-1)\sin(2\Delta k_z z)}{(1+D^2-2D\cos(2\Delta k_z z))^2}. \quad (7)$$

3. Results

We produced these beams using diffraction from nanofabricated holograms, such as the one shown in figure 3. The hologram was placed in the front focal plane of a lens (one focal length before the lens) system in a TEM, such that the Fourier transform of the hologram occurred in the Fourier plane of the lens (one focal length after the lens). The TEM was adjusted to demagnify and project an image of this diffracted electron pattern onto a

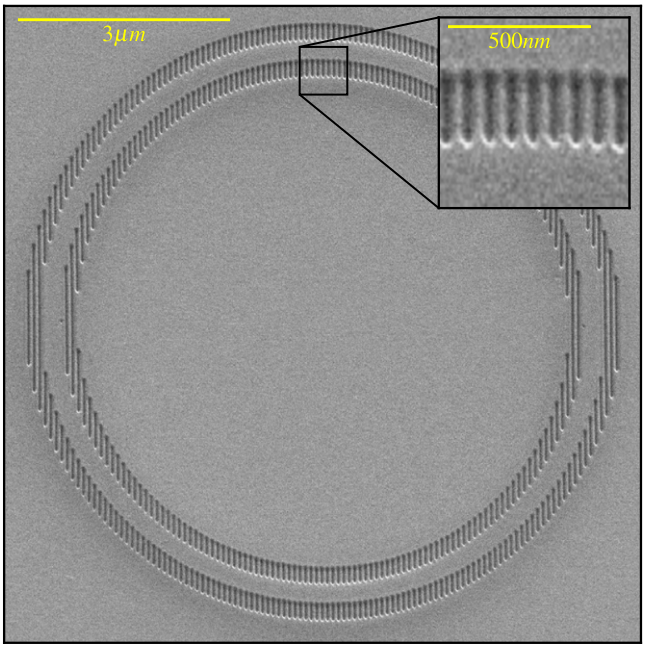

Figure 3. Hologram. Our hologram is placed in the front focal plane of a lens (a focal length before the lens) and consists of a double ring slit of differing radii, producing an accelerating wave in the Fourier plane (a focal length after the lens) (see Supplementary Information). Each ring is designed to produce a non-canonical Bessel vortex beam from a superposition of two canonical Bessel vortex beams.

pixelated imaging detector. The focal conditions of this imaging system were adjusted such that the beam could be imaged at various locations along the optical axis.

The design and fabrication method of the hologram is explained in more detail in the supplementary information, which is available online at stacks.iop.org/NJP/21/043018/mmedia. The Fourier transform $\mathcal{F}[\psi(\mathbf{r})]$ of the desired wave was encoded onto the hologram using an off-axis design, which encodes the phase using a sinusoidal carrier. The Fourier transform of a single Bessel mode, $\mathcal{F}[\psi(\mathbf{r})] = \mathrm{e}^{\mathrm{i}\ell\phi}\delta(r - r')$, forms an azimuthal phase around a ring of infinitesimal thickness we call a 'delta' ring. The azimuthal phase, when encoded by a sinusoidal carrier, results in a two-dimensional sinusoidal pattern featuring a fork dislocation [10]. In an actual hologram, the delta ring must have a finite thickness in order to host the sinusoidal carrier and diffract a reasonable electron current into the desired beam. However, the non-zero ring thickness approximating the radial delta function results in a diffracted beam of finite width, which affects the quality of the generated Bessel beam and the focal range over which it is approximately Bessel-like. Thus we chose a width such that the diffracted beam was very close to a true Bessel beam within the experimental focal range, while still having sufficient intensity. To create the twisting electron beam composed of superpositions of Bessel beams, the hologram was designed with two distinct delta rings with a slightly different r' parameter. The thickness of each ring is 200 nm, while the diameter of the rings is 8.0 and 7.0 μm. To separate the diffracted beams, the period of the carrier wave is 75 nm. The relatively small diameter of the holograms was chosen so that the resulting diffracted beam would be large enough in our detector to observe the detail of the beam. With this hologram we are able to observe spiralling electron waves for the first time, as shown in figure 1. The results are shown for the $\ell = \pm 1$ superposition of non-canonical vortex beams.

To determine the angular velocity and acceleration, images of the beam's intensity profile were taken for $\ell = 1$ and $D = 0, 0.158, 0.325$, and 0.510 at equally spaced locations along the optical axis in a focal series. The angular orientation of the probability distribution was extracted from these images, with the results shown in figure 4. The anisotropic parameter that we encoded into the diffraction grating is given by D_{exp} in the figures and serves as the 'expected' anisotropic parameter, while D_{fit} is retrieved by fitting equation (5) to the data and retrieving the D parameter from this fit. The expected and fitted acceleration points align very closely. We note that small changes in D make almost imperceptible differences in the rotation unless D is close to one, as seen in the difference between the fitted and predicted curves in figure 4. With these considerations in mind, we claim that the measured values given by D_{fit} align well with the encoded D_{exp}. Our measured velocity and acceleration closely match with the predicted data, as shown in figure 5. The data represented in figure 4 was used to reconstruct the three-dimensional structure of the beam shown in figure 1.

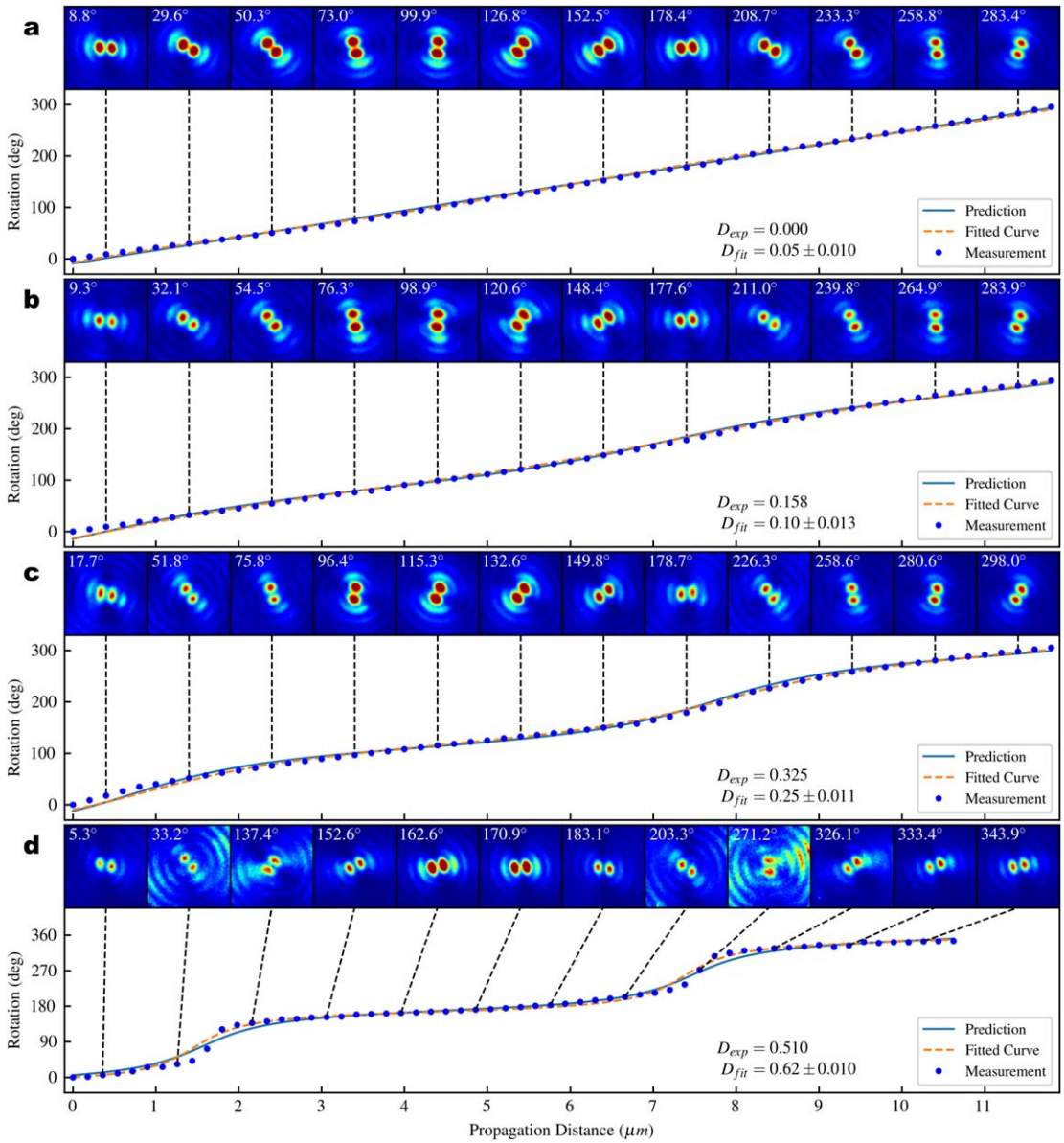

Figure 4. Rotating matter waves. Experimental results for the rotation of the matter waves as a function of propagation distance. D_{exp} is the encoded anisotropic parameter on our hologram while D_{fit} is the calculated parameter from the data. The theoretical (blue curve), fitted (orange curve) and measured rotation (points) are plotted together for comparison for the cases of (a) $D_{\mathrm{exp}} = 0$, (b) $D_{\mathrm{exp}} = 0.158$, (c) $D_{\mathrm{exp}} = 0.325$, and (d) $D_{\mathrm{exp}} = 0.510$. The insets show the measured detected electron distributions with the white text the measured rotation of wave relative to the first frame in the sequence.

4. Discussion

The energy flow associated with spontaneous angular accelerations of electron matter waves can be understood by considering the probability current distribution, $\mathbf{j} = -\mathrm{i}\hbar\,(\psi^*\nabla\psi - \psi\nabla\psi^*)/2m$. The vectorial component of the waves' probability current density, and thus the momentum trajectories inside the wave, can be attributed to the gradient of its phase. That is, for a wavefunction ψ, the corresponding current density satisfies $\mathbf{j} \propto \nabla \arg\,\psi$, where $\arg\,\psi$ refers to the argument or the phase of the wavefunction [31]. The phase of the angularly accelerating wavefunction (equation (3)) is given by:

$$\arg\,\psi_{acc} = \arctan\left(\frac{J_\ell(k_{r1}r) - J_\ell(k_{r2}r)}{J_\ell(k_{r1}r) + J_\ell(k_{r2}r)}\tan(\Delta k_z z + \ell\varphi_\ell(\phi))\right). \tag{8}$$

The above equation only yields values of 0 and π. This reveals that the two intertwined lobes in the accelerating wavefunction are π out of phase. Despite an apparent helical probability current density, we find that the transverse gradient of the phase is zero everywhere, and thus the current lines correspond to straight trajectories in the longitudinal direction, as shown in figure 6(a). To emphasize this claim, we simulate the propagation of a wave ψ_{acc} where $\ell = 1$ and $D = 0.5$ through an aperture aligned such that one of the main lobes of the wave's

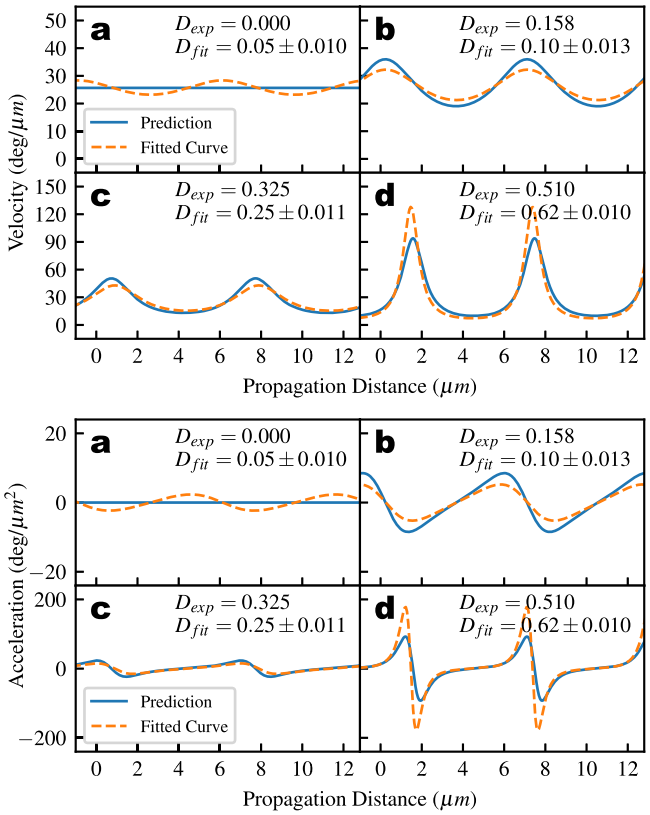

Figure 5. Measured angular velocity and acceleration. (Top) The measured velocity of the wave as it propagates and (Bottom) the measured acceleration of the wave as it propagates. All results are shown for (a) $D_{\text{exp}} = 0$, (b) $D_{\text{exp}} = 0.158$, (c) $D_{\text{exp}} = 0.325$ and (d) $D_{\text{exp}} = 0.510$. The solid blue curve is the theoretical result based on the programmed hologram (D_{exp}) shown together with the orange dashed curve from the measured data (D_{fit}).

probability density passes through it. The results of these simulations are shown in figure 6 (b), where we observe that the wave ceases rotating once it goes through the aperture.

We also model the electric and magnetic fields emanating from these matter waves. We adopt a semiclassical model in which we equate the waves' electric charge $\rho_e(\mathbf{r})$ and current $\mathbf{j}_e(\mathbf{r})$ densities to their probability densities [2]. Explicitly, we let $\rho_e(\mathbf{r}) = \mathrm{e}\rho(\mathbf{r})$ and $\mathbf{j}_e(\mathbf{r}) = \mathrm{e}\,\mathbf{j}(\mathbf{r})$, where e is the electron's charge, $\rho(\mathbf{r}) = |\psi(\mathbf{r})|^2$. Here we consider a more realistic model of a coiling electron wavepacket of finite extent in both longitudinal and transverse directions. The finite energy spread of the electrons is accounted for by modulating the longitudinal component of our wavefunctions by a Gaussian function. We also replace any occurrences of Bessel wavefunctions by Bessel–Gauss solutions [32] to the Schrödinger equation, which account for the propagation of Bessel waves modulated by a radial Gaussian function. We numerically compute the electromagnetic potentials due to these charge and current distributions, and derive the resulting electric and magnetic fields.

In figure 6 (c), we consider the case of a finite version of the accelerating wave introduced in equation (3), where we let $k_{z2} = 2k_{z1}, \ell = 1$, and $D = 0.5$. For both cases, we can see that the radial components of the waves' Poynting vector, which is proportional to $\mathbf{E} \times \mathbf{B}$, scales down faster than r^2 thus implying that the wave's static fields do not lead to radiation.

5. Conclusion

We have demonstrated a twisted electron beam with a rotating intensity distribution within the cavity of a TEM. In addition to producing lobed charge distributions that rotate constantly in time without an external field, we also demonstrate charge distributions that periodically exhibit angular acceleration. While this behavior has been demonstrated before in beams of light, it is not immediately obvious that the same local angular accelerations can be produced in beams of charged, massive particles. Indeed, classical physics prohibits such behavior. Our result is understood by considering that the each electron is described by a symmetric matter wave, the centroid of which does not accelerate, and the rotations and angular accelerations of individual components of this wavefunction are local in nature. The angular velocity and acceleration of the field could be inferred and showed good agreement with the theoretical predictions. The results challenge conventional

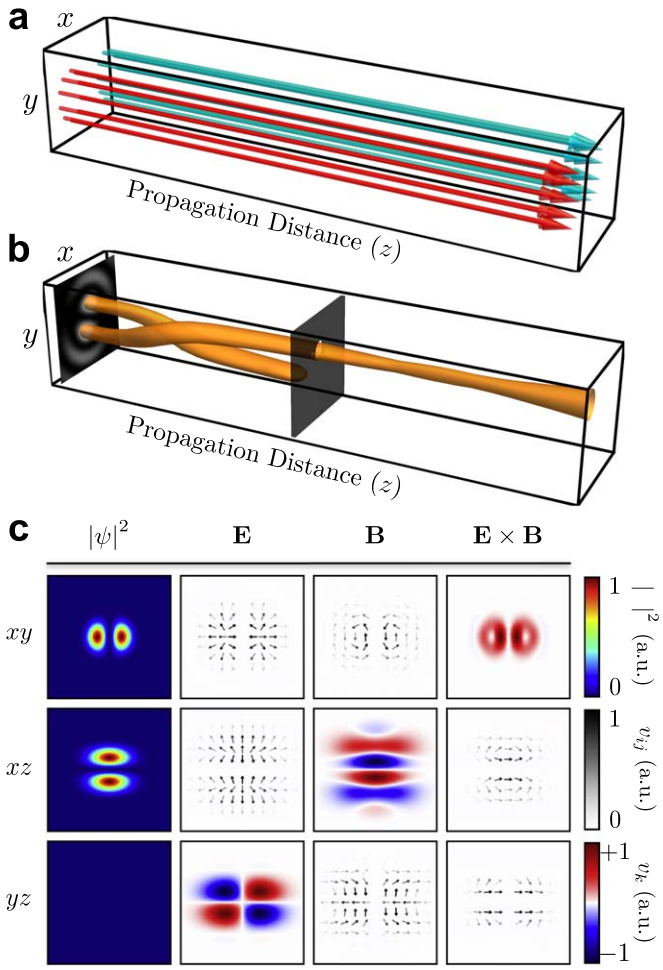

Figure 6. Semiclassical dynamics and electromagnetic fields of angularly accelerating electron waves. (a) Current lines of an angularly accelerating wavefunction which, in this case, correspond to the wave's ray optics classical trajectories. The arrows form a contour of the wave's probability density at the focal plane and are colored based on the phase at the corresponding points, illustrating the two-lobed structure. In the limit where the two converging waves forming the spiralling distribution have very similar convergence angles α, then there are no phase gradients in the wave's profile. Therefore, the probability current lines are straight and they correspond to the electron's classical trajectories. (b) Simulated behavior of an angularly accelerating electron wave upon propagating through an aperture and where k_{z1} and k_{z2} are scaled to observe diffraction related effects. The shown surfaces are defined by the half-maximum value of the wave's maximum probability density in a given plane. (c) Probability density ($|\psi|^2$) of a coiling electron wavepacket, where $\ell = 1$ and $D = 0.5$, shown in the *xy*, *xz*, and *yz* plane. Its static electric (**E**) and magnetic (**B**) fields along with their cross product are also shown. The vectorial component that is transverse to the plane, v_{ij} (v_{xy}, v_{xz}, v_{yz}), is show as black arrows plotted on top of the perpendicular component, v_k (v_z,v_y, v_x). The opacity of the arrows and the scheme's intensity are jointly normalized to faithfully represent the relative magnitudes of each vector component.

notions of rotational kinetics but the paradoxes it raises can be resolved by a simple model of the electron as an extended wavefunction, thus providing deeper insight in angular motion.

Our work introduces a new class of matter wave based on controlling the angular acceleration of an electron's wavefunction in a predictable manner. Earlier reported electron vortex states undergo only partial orbits and can be described by straight trajectories of classical particles [2, 10]; their helical structure only represents the timing of the wave, whereas here we demonstrate electron states with actual winding probability current density. A series of previous investigations showed that the OAM degree of freedom of electron wavefunctions in a longitudinal magnetic field can couple to Landau states, which can result in a nonuniform angular rotation through nearly 90° [33–36], but the size of the beam changes as well and the authors note that this behavior can be described by classical charged particles following ray trajectories within an external field. The Gouy phase may also be used to rotate beams and has been demonstrated in the optical [29] and matter wave [33] regimes. Our work here differs in these previous approaches in that we demonstrate rapidly coiling currents in free space devoid of an external fields, in a beam that does not change size. Furthermore, unlike previous works, our approach allows for the angular acceleration to be tuned in a controllable way both in magnitude and over an extended distance.

In addition to providing a rich new system to explore OAM in the quantum regime, the rotating electron beams could potentially be used for several applications. There have been reports of using canonical electron

vortex beams to rotate nanoparticles on dry substrates [37, 38] as well as in liquid environments [39]. In optical traps, coiling light beams have been used to create multiple traps that can each manipulate microparticles [40]. Perhaps these technique can now be combined to manipulate multiple particles at the nanoscale. Furthermore, self-coiling electron beams could provide a rich system to explore resonance conditions high-power beam systems, such as helical undulators in a synchrotron or free electron laser, or inside high power vacuum electronics.

Acknowledgments

AF acknowledges financial support from the South African National Research Foundation; BJM and JSP acknowledge support by the National Science Foundation under Grant No. 1607733 and partial support by the US Department of Energy, Office of Science, Basic Energy Sciences, under Award DE-SC0010466. HL and EK acknowledge support from the Canada Research Chairs. The authors would like to thank Melanie McLaren, Elias Sideras-Haddad, and Vincenzo Grillo for useful discussions.

ORCID iDs

A Forbes https://orcid.org/0000-0003-2552-5586

References

[1] Harris J, Grillo V, Mafakheri E, Gazzadi G C, Frabboni S, Boyd R W and Karimi E 2015 *Nat. Phys.* **11** 629–34
[2] Bliokh K Y *et al* 2017 *Phys. Rep.Phys. Rep.* **690** 1–70
[3] Lloyd S M, Babiker M, Thirunavukkarasu G and Yuan J 2017 *Rev. Mod. Phys.* **89** 035004
[4] Larocque H, Kaminer I, Grillo V, Leuchs G, Padgett M J, Boyd R W, Segev M and Karimi E 2018 *Contemp. Phys.* **0** 1–19
[5] Dirac P A M 1931 *Proc. R. Soc. A* **133** 60–72
[6] McMorran B J, Agrawal A, Ercius P A, Grillo V, Herzing A A, Harvey T R, Linck M and Pierce J S 2017 *Phil. Trans. R. Soc. A* **375** 20150434
[7] Uchida M and Tonomura A 2010 *Nature* **464** 737–9
[8] Sueda K, Miyaji G, Miyanaga N and Nakatsuka M 2004 *Opt. Express* **12** 3548–53
[9] Verbeeck J, Tian H and Schattschneider P 2010 *Nature* **467** 301–4
[10] McMorran B J, Agrawal A, Anderson I M, Herzing A A, Lezec H J, McClelland J J and Unguris J 2011 *Science* **331** 192–5
[11] Harvey T R, Pierce J S, Agrawal A K, Ercius P, Linck M and McMorran B J 2014 *New J. Phys.* **16** 093039
[12] Grillo V, Karimi E, Gazzadi G C, Frabboni S, Dennis M R and Boyd R W 2014 *Phys. Rev.* X **4** 011013
[13] Fukuhara A, Shinagawa K, Tonomura A and Fujiwara H 1983 *Phys. Rev.* B **27** 1839–43
[14] Tonomura A 1987 *Rev. Mod. Phys.* **59** 639–69
[15] Beche A, Van Boxem R, Van Tendeloo G and Verbeeck J 2014 *Nat. Phys.* **10** 26–9
[16] Lloyd S M, Babiker M and Yuan J 2012 *Phys. Rev.* A **86** 023816
[17] Rusz J and Bhowmick S 2013 *Phys. Rev. Lett.* **111** 105504
[18] Grillo V *et al* 2017 *Nat. Commun.* **8** 689
[19] Verbeeck J, Schattschneider P, Lazar S, Stöger-Pollach M, Löffler S, Steiger-Thirsfeld A and Van Tendeloo G 2011 *Appl. Phys. Lett.* **99** 203109
[20] Lloyd S, Babiker M and Yuan J 2012 *Phys. Rev. Lett.* **108** 074802
[21] Berry M V and McDonald K T 2008 *J. Opt. A: Pure Appl. Opt.* **10** 035005
[22] Gori F, Guattari G and Padovani C 1987 *Opt. Commun.* **64** 491–5
[23] Molina-Terriza G, Wright E M and Torner L 2001 *Opt. Lett.* **26** 163–5
[24] Vasilyeu R, Dudley A, Khilo N and Forbes A 2009 *Opt. Express* **17** 23389–95
[25] Chávez-Cerda S, McDonald G and New G 1996 *Opt. Commun.* **123** 225–33
[26] Pääkkönen P, Lautanen J, Honkanen M, Kuittinen M, Turunen J, Khonina S N, Kotlyar V V, Soifer V A and Friberg A T 1998 *J. Mod. Opt.* **45** 2355–69
[27] Rop R, Dudley A, López-Mariscal C and Forbes A 2012 *J. Mod. Opt.* **59** 259–67
[28] Schulze C, Roux F S, Dudley A, Rop R, Duparré M and Forbes A 2015 *Phys. Rev.* A **91** 043821
[29] Webster J, Rosales-Guzmán C and Forbes A 2017 *Opt. Lett.* **42** 675–8
[30] Maji S and Brundavanam M M 2017 *Opt. Lett.* **42** 2322–5
[31] Berry M V and McDonald K 2008 *J. Opt. A: Pure Appl. Opt.* **10** 035005
[32] Bagini V, Frezza F, Santarsiero M, Schettini G and Spagnolo G S 1996 *J. Mod. Opt.* **43** 1155–66
[33] Schachinger T, Löffler S, Stöger-Pollach M and Schattschneider P 2015 *Ultramicroscopy* **158** 17–25
[34] Bliokh K Y, Schattschneider P, Verbeeck J and Nori F 2012 *Phys. Rev.* X **2** 041011
[35] Guzzinati G, Schattschneider P, Bliokh K Y, Nori F and Verbeeck J 2013 *Phys. Rev. Lett.* **110** 093601
[36] Schattschneider P, Schachinger T, Stöger-Pollach M, Löffler S, Steiger-Thirsfeld A, Bliokh K Y and Nori F 2014 *Nat. Commun.* **5** 4586
[37] Gnanavel T, Yuan J and Babiker M 2012 Observation of gold nanoparticles movements under sub-10nm vortex electron beams in an aberration corrected TEM *Royal Microscopical Society: Proc. European Microscopy Congress (Proc. EMC 2012)* ed D J Stokes and J Hutchison
[38] Verbeeck J, Tian H and Van Tendeloo G 2013 *Adv. Mater.* **25** 1114–7
[39] Greenberg A, DeVyldere H, Pierce J and McMorran B 2018 *Proc. SPIE* **10723** 107231O
[40] Grier D G 2003 *Nature* **424** 810